

Article

# Structural Phase Transition and Compressibility of CaF<sub>2</sub> Nanocrystals under High Pressure

Jingshu Wang <sup>1</sup> , Jinghan Yang <sup>1</sup>, Tingjing Hu <sup>1</sup> , Xiangshan Chen <sup>1</sup>, Jihui Lang <sup>1,\*</sup>, Xiaoxin Wu <sup>1</sup>, Junkai Zhang <sup>1</sup>, Haiying Zhao <sup>1</sup>, Jinghai Yang <sup>1</sup> and Qiliang Cui <sup>2</sup>

<sup>1</sup> Key Laboratory of Functional Materials Physics and Chemistry of the Ministry of Education, National Demonstration Center for Experimental Physics Education, Jilin Normal University, Siping 136000, China; wjs@jlnu.edu.cn (J.W.); jlsfdxchina@163.com (J.Y.); tjhumars@126.com (T.H.); 13134497345@163.com (X.C.); wuXiaoxin@126.com (X.W.); junkaizhang126@126.com (J.Z.); HaiyingZh@126.com (H.Z.); jhyang1@jlnu.edu.cn (J.Y.)

<sup>2</sup> State Key Laboratory of Superhard Materials, Jilin University, Changchun 130012, China; wjs\_916\_82@126.com

\* Correspondence: langjihui80@126.com

Received: 19 March 2018; Accepted: 26 April 2018; Published: 3 May 2018



**Abstract:** The structural phase transition and compressibility of CaF<sub>2</sub> nanocrystals with size of 23 nm under high pressure were investigated by synchrotron X-ray diffraction measurement. A pressure-induced fluorite to  $\alpha$ -PbCl<sub>2</sub>-type phase transition starts at 9.5 GPa and completes at 20.2 GPa. The phase-transition pressure is lower than that of 8 nm CaF<sub>2</sub> nanocrystals and closer to bulk CaF<sub>2</sub>. Upon decompression, the fluorite and  $\alpha$ -PbCl<sub>2</sub>-type structure co-exist at the ambient pressure. The bulk modulus  $B_0$  of the 23 nm CaF<sub>2</sub> nanocrystals for the fluorite and  $\alpha$ -PbCl<sub>2</sub>-type phase are 103(2) and 78(2) GPa, which are both larger than those of the bulk CaF<sub>2</sub>. The CaF<sub>2</sub> nanocrystals exhibit obviously higher incompressibility compare to bulk CaF<sub>2</sub>. Further analysis demonstrates that the defect effect in our CaF<sub>2</sub> nanocrystals plays a dominant role in the structural stability.

**Keywords:** high pressure; CaF<sub>2</sub> nanocrystals; phase transitions; X-ray; bulk modulus

## 1. Introduction

Calcium fluoride (CaF<sub>2</sub>)—with low absorption coefficient, high transmittance, anionic conductivity, and high resistivity—has become the focus of fundamental scientific research and industrial applications [1–3]. Especially because of its typical crystal structure, CaF<sub>2</sub> becomes the best material for high pressure research. At ambient conditions, bulk CaF<sub>2</sub> crystallizes in the cubic fluorite structure ( $Fm\bar{3}m$ ), in which Ca and F atoms occupy Wyckoff position 4a and 8c positions, respectively. Many theoretical and experimental studies on structural phase transition, optical, and electronic properties of CaF<sub>2</sub> under high pressure have been reported [4–13]. At high pressure, CaF<sub>2</sub> undergoes two structural phase transitions to highly coordinated structures. The first phase transition from the fluorite structure to an orthorhombic  $\alpha$ -PbCl<sub>2</sub>-type structure ( $Fm\bar{3}m$  to  $Pnma$ ) is reported to occur at 8–10 GPa [4–6]. Theoretical studies of CaF<sub>2</sub> predicted that the second phase transition from  $\alpha$ -PbCl<sub>2</sub>-type structure to Ni<sub>2</sub>In-type structure ( $Pnma$  to  $P6_3/mmc$ ) takes place at 68–278 GPa [6,7]. Experimental research by S M Dorfman et al. reported that bulk CaF<sub>2</sub> transformed from the  $\alpha$ -PbCl<sub>2</sub>-type structure to the Ni<sub>2</sub>In-type structure at 79 GPa with heating to about 2000 K [8]. Although there are widely high-pressure studies on bulk CaF<sub>2</sub>, yet very few experimental studies on nanosized CaF<sub>2</sub> exist for comparison.

Because of the surface effect and quantum confinement effect yielded by the significantly decrease in size, applications of high pressure have proven to be an important tool in tailoring the properties of

nanomaterials [14–33]. Previous high-pressure studies on nanomaterials have revealed a set of novel high-pressure behaviors, which differ from that of their corresponding bulk materials. The size effect has a great influence on the phase transition pressure [16–19], the course of amorphization [21–25], and phase transition routines [26]. Our previous high-pressure X-ray diffraction study revealed that CaF<sub>2</sub> nanocrystals with size of 8 nm transformed from fluorite structure into  $\alpha$ -PbCl<sub>2</sub>-type structure at 14 GPa, and the high-pressure structure was stable up to 46.5 GPa. The enhancement of structural stability is mainly due to the surface energy differences between the cubic and orthorhombic phases [34]. Beyond that, pressure-induced structural transition of nanosized CaF<sub>2</sub> has no other reports, and the bulk modulus of nanoscale CaF<sub>2</sub> is still not well known. In order to further research the high-pressure behaviors of nanosized CaF<sub>2</sub>, and explore the important factors to affect the structural stability of nanomaterials, more experimental data for various sized CaF<sub>2</sub> is urgently needed.

Herein, we present our observations on structural phase transition and compressibility of 23 nm CaF<sub>2</sub> nanocrystals using synchrotron X-ray diffraction measurement. We found that the phase-transition pressure from fluorite to  $\alpha$ -PbCl<sub>2</sub>-type is lower than that previously reported of 8 nm CaF<sub>2</sub> nanocrystals and closer to bulk CaF<sub>2</sub>. The bulk modulus of the 23 nm CaF<sub>2</sub> nanocrystals for the fluorite and  $\alpha$ -PbCl<sub>2</sub>-type structure are both larger than those of the bulk CaF<sub>2</sub>. We believe that the enhancement of bulk modulus is due to higher surface energy. We observed that the as-synthesized CaF<sub>2</sub> nanocrystals contain visible dislocations and defects which could play a dominant role in structural stability.

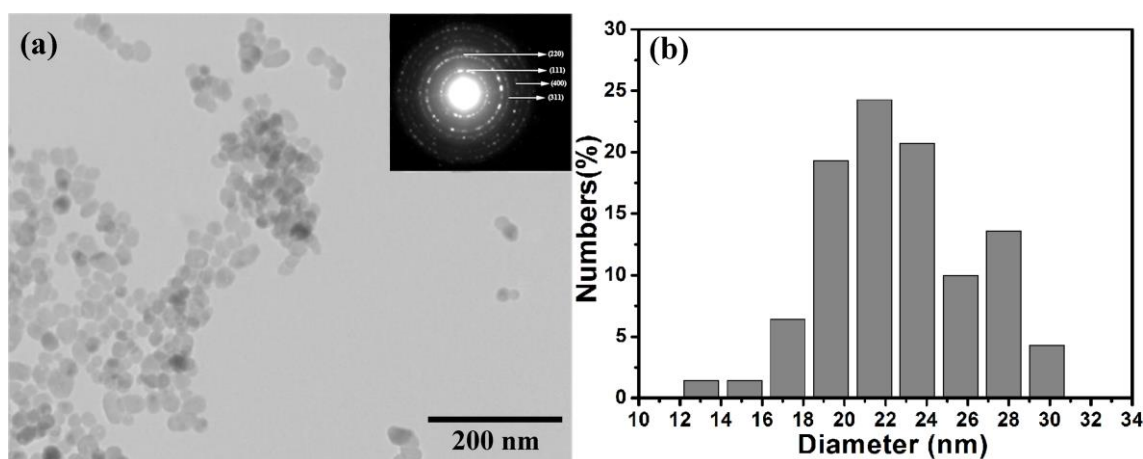
## 2. Materials and Methods

The 23 nm-sized CaF<sub>2</sub> nanocrystals were synthesized using the solvothermal synthesis method. 0.5 mmol of Ca(NO<sub>3</sub>)<sub>2</sub> and 1 mmol of NaF were dissolved in 10 mL distilled water to form clear solutions, respectively. The two solutions were mixed under full stirring to obtain opaque white suspension. The solution was transferred in to a 40ml autoclave which was filled to 85% of its total capacity with ethanol. Then, the system was kept in an oven at 140 °C for 15 h and cooled in air naturally. The final products were obtained after centrifugation and drying treatment.

The crystalline morphology and particle size of synthesized CaF<sub>2</sub> nanocrystals were examined by transmission electron microscopy TEM (200 KV, H-8100IV; HITACHI, Tokyo, Japan) and high-resolution transmission electron microscopy HRTEM (JEM-2100HR; JEOL, Tokyo, Japan). The sample was loaded into a symmetric diamond anvil cell (DAC) with a culet size of 300  $\mu$ m for high-pressure characterization, and silicon oil was chosen as the pressure transmitting media. The synthesized CaF<sub>2</sub> nanocrystals were enclosed into a 100- $\mu$ m-diameter hole of the T301 stainless steel gasket. The shift of the ruby R1 line was utilized to calibrate the pressure. A high-pressure X-ray diffraction experiment was performed at BL15U stations of Shanghai Synchrotron Radiation Facility26 (SSRF,  $\lambda = 0.6199$  Å). A focused beam size of  $3 \times 3$   $\mu$ m<sup>2</sup> was used for data collection. MAR165 CCD detector was utilized to collect the X-ray diffraction data. The distance between the sample and CCD detectors was 173 mm which was calibrated using a CeO<sub>2</sub> standard. FIT2D software was used to process the two-dimensional X-ray diffraction images. The ORIGIN8 and MATERIAL STUDIO programs were adopted to refine high-pressure synchrotron XRD patterns.

## 3. Results and Discussion

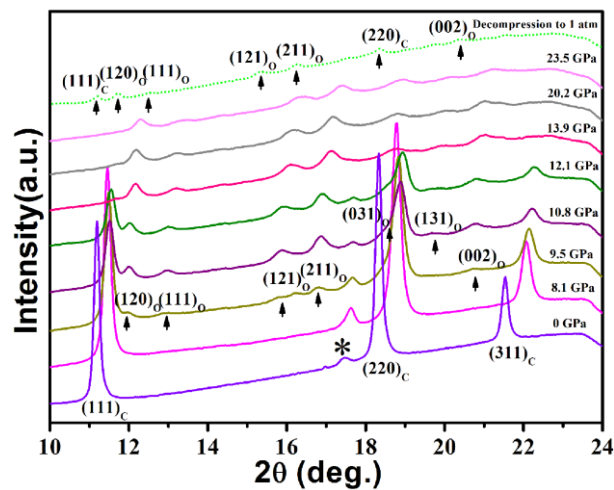
Figure 1 shows that the shape of as-prepared CaF<sub>2</sub> nanocrystals is irregular particle with uniform morphology. Selected-area electron diffraction (SAED) pattern (inset in Figure 1a) shows that the major diffraction rings can be indexed into a cubic structure. Figure 1b displays the corresponding particle size distribution histograms. The distribution is narrow, and the average size is  $23 \pm 4$  nm.



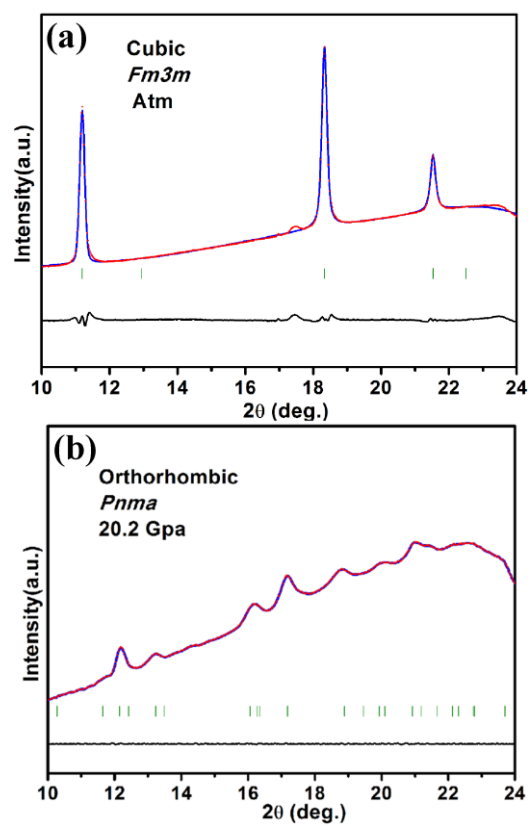
**Figure 1.** (a) TEM image of the as-synthesized CaF<sub>2</sub> nanocrystals. Inset in (a) represents the corresponding SAED pattern. (b) Particle size distribution of CaF<sub>2</sub> nanocrystals.

Figure 2b presents XRD spectra for the 23 nm CaF<sub>2</sub> nanocrystals collected by increasing the pressure gradually up to 23.5 GPa. Starting at ambient pressure, three diffraction peaks of CaF<sub>2</sub> nanocrystals together with one peak of the gasket material (marked by star) are observed. As shown in Figure 3a, the Rietveld refinement performed at ambient pressure suggests that the nanocrystals diffraction peaks is in a good agreement with belong to the fluorite structure with space group of *Fm3m* (*Rwp* = 0.98%, *Rp* = 0.62%). The fluorite structure was characterized by ‘Ca’ and ‘F’ atoms occupying the (0, 0, 0) and (0.25, 0.25, 0.25) position, respectively. We can clearly observe that a phase transition from fluorite structure to  $\alpha$ -PbCl<sub>2</sub>-type structure takes place at 9.5 GPa. This phase-transition pressure is lower than that the previously reported 8 nm CaF<sub>2</sub> nanocrystals and closes to bulk CaF<sub>2</sub>. At pressures higher than 9.5 GPa, additional diffraction new peaks emerge and intensity increases with increasing pressure. At the same time, the diffraction peaks representing the cubic phase become weak. Figure 4 shows the unit-cell parameters as function of pressure. At 9.5 GPa, the cell parameter and unit cell volume of cubic structure were calculated to be  $a = 5.35(9) \text{ \AA}$  and  $V = 153.93 (3) \text{ \AA}^3$ . Meanwhile, we obtain the cell parameters and unit cell volume of the  $\alpha$ -PbCl<sub>2</sub>-type structure ( $a = 6.90(1)$ ,  $b = 5.83(7) \text{ \AA}$ ,  $c = 3.45(6) \text{ \AA}$ , and  $V = 139.18 (5) \text{ \AA}^3$ ). The volume change for the fluorite and  $\alpha$ -PbCl<sub>2</sub>-type structures is a decrease of 9.6% from the low-pressure structure. Complete phase transformation to the high-pressure phase occurs at 20.2 GPa. It is clearly observed that the cubic fluorite structure still exists in the 10–20 GPa range after the phase-transition pressure at 9.5 GPa. The phase transformation is quite sluggish. The Rietveld refinement performed at 20.2 GPa shows that the XRD experimental datum is in a great agreement with an  $\alpha$ -PbCl<sub>2</sub>-type cell with space group *Pnma* (*Rwp* = 1.09%, *Rp* = 1.07%) with the unit cell volume of  $129.95 (2) \text{ \AA}^3$  (Figure 3b). The Ca and F ions of the  $\alpha$ -PbCl<sub>2</sub>-type structure occupy the positions Ca(0.253, 0.25, 0.109), F1(0.859, 0.25, 0.073), and F2 (0.438, 0.25, 0.834), respectively. The high-pressure  $\alpha$ -PbCl<sub>2</sub>-type structure can be maintained up to the highest studied pressure of 23.5 GPa in our XRD measurements.

Upon decompression, the original fluorite phase of 23 nm CaF<sub>2</sub> nanocrystals is not recovered when the pressure is reduced to 8.4 GPa. The experimental data point that the transition from orthorhombic to cubic phase exhibits strong hysteresis under decompression. After decompression to ambient condition, the sample retains the  $\alpha$ -PbCl<sub>2</sub>-type structure with for the peaks attributed to fluorite structure remain in the XRD datum. It indicates that the fluorite and  $\alpha$ -PbCl<sub>2</sub>-type structure co-exist at the ambient pressure after decompression. This result is in good accordance with the reports on the bulk CaF<sub>2</sub> [4], and the hysteresis might be explained as the inherent sluggish nature of CaF<sub>2</sub>. For the reported 8 nm-sized CaF<sub>2</sub> nanocrystals, the high-energy hindrance prevents the transition to the fluorite structure which might be the reason for irreversibility at ambient pressure.



**Figure 2.** High-pressure X-ray diffraction patterns of  $\text{CaF}_2$  nanocrystals. Upon being completely quenched to the ambient conditions. The peak (marked with asterisk) is derived from the T301 stainless steel gasket.



**Figure 3.** Refinements of the experiment (red dots), simulation (blue line), and difference (black line) ADXRD patterns of fluorite ( $Fm\bar{3}m$ ) and  $\alpha\text{-PbCl}_2$ -type ( $Pnma$ ) phase: (a) at ambient pressure; (b) at 20.2 GPa. Green bars mark the positions of corresponding Bragg reflections.

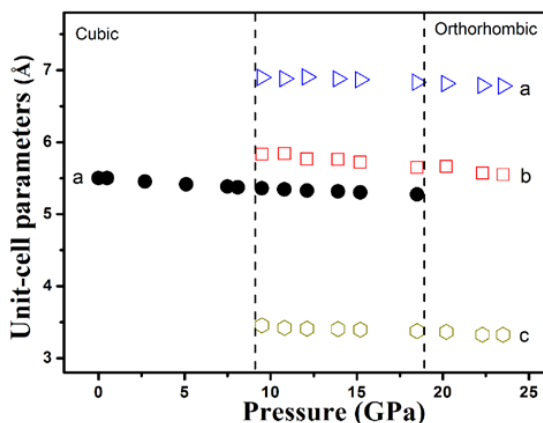


**Figure 4.** Pressure dependence of the lattice parameters in CaF<sub>2</sub> nanocrystals. Filled symbols denote cubic fluorite structure. Open symbols denote the orthorhombic PbCl<sub>2</sub>-type structure.

Figure 5 demonstrates the EOS data of CaF<sub>2</sub> nanocrystals to pressures of 23.5 GPa. A third-order Birch-Murnaghan (BM) equation of state (EOS) was fitted to the experimental *P–V* data [35].

$$P = (3/2)B_0[(V/V_0)^{-7/3} - (V/V_0)^{-5/3}]\{1 + (3/4)(B_0' - 4) \times [(V/V_0)^{-2/3} - 1]\} \tag{1}$$

where *V* and *V*<sub>0</sub> are the volumes at pressure *P* given in GPa and ambient pressure, respectively. For the CaF<sub>2</sub> nanocrystals, we yield the bulk modulus *B*<sub>0</sub> of 103(2) GPa with *B*<sub>0</sub>' fixed at 5 for the fluorite structure and *B*<sub>0</sub> of 78(2) GPa with *B*<sub>0</sub>' fixed at 4 for the α-PbCl<sub>2</sub>-type structure. The isothermal bulk modulus of α-PbCl<sub>2</sub>-type phase at ambient pressure is lower than the fluorite phase. The lower bulk modulus at high pressure indicates higher compressibility of the high-pressure phase of CaF<sub>2</sub> nanocrystals. This result is consistent with previous studies on bulk CaF<sub>2</sub>, but it is different from bulk SrF<sub>2</sub> and BaF<sub>2</sub>, which have higher incompressibility under high pressure [8,36]. The bulk modulus of CaF<sub>2</sub> nanocrystals for the fluorite and α-PbCl<sub>2</sub>-type structure are both significantly larger than those of the bulk CaF<sub>2</sub> (*B*<sub>0</sub> = 87(5) and 74(5) GPa) [4,8], indicating the high incompressibility of nanosized CaF<sub>2</sub>.

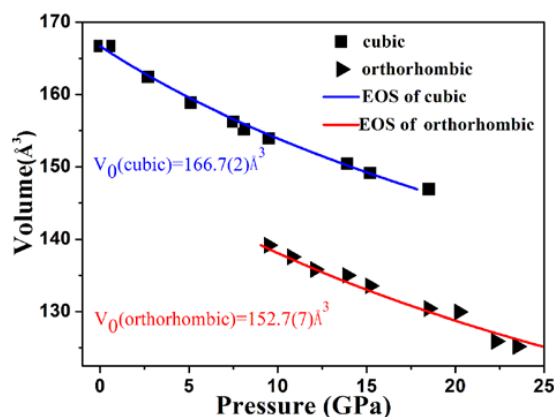


**Figure 5.** Unit-cell volume as a function of pressure determined for the CaF<sub>2</sub> nanocrystals. Solid curves are the Birch–Murnaghan EOS fits to the experimental data.

Table 1 exhibits the phase transition (*P*<sub>T</sub>) starting pressure and the values of *B*<sub>0</sub> and *B*<sub>0</sub>' of CaF<sub>2</sub> materials, which clearly revealed the differences between bulk and nanoscale CaF<sub>2</sub>. It was found that the high-pressure behavior of the 23 nm CaF<sub>2</sub> nanocrystals is closer to that in bulk CaF<sub>2</sub>. However, the bulk modulus of the CaF<sub>2</sub> nanocrystals for the fluorite and α-PbCl<sub>2</sub>-type structure are both larger than those of the bulk CaF<sub>2</sub>. This indicates that the CaF<sub>2</sub> nanocrystals exhibit obviously higher

incompressibility compared to bulk  $\text{CaF}_2$ . This behavior is different from the results reported for nanocrystalline  $\text{SnO}_2$  and  $\text{TiO}_2$  [37,38]. Compared with bulk  $\text{CaF}_2$ , a relatively higher surface energy is expected in our  $\text{CaF}_2$  nanocrystals. Based on the Hall–Petch effect [39,40], a continuous decrease of grain size could further elevate material hardness, and thus the enhancements in bulk modulus can be easily understood.

**Table 1.** Transition pressure ( $P_T$ ), and equation of state parameters ( $B_0$  and  $B_0'$ ) of fluorite-type and  $\alpha\text{-PbCl}_2$ -type  $\text{CaF}_2$

Morphology	Size	$P_T$ (GPa)	$B_0$ (GPa)		$B_0'$	
			<i>Fm3m</i>	<i>Pnma</i>	<i>Fm3m</i>	<i>Pnma</i>
Bulk	Micro	9.5 <sup>1</sup>	87(5) <sup>1</sup>	74(5) <sup>2</sup>	5	4.7
		9 <sup>3</sup>	81(1) <sup>3</sup>	–	5.22	–
		8.1 <sup>4</sup>	79.54 <sup>4</sup>	70.92 <sup>4</sup>	4.54	4.38
Nanocrystals	8 nm	14 <sup>5</sup>	–	–	–	–
This work	23 nm	9.5	103(2)	78(2)	5	4

<sup>1</sup> Ref. [4]; <sup>2</sup> Ref. [8]; <sup>3</sup> Ref. [41]; <sup>4</sup> Ref. [6]; <sup>5</sup> Ref. [34].

Extensive high pressure studies indicated that many nanomaterials—such as  $\text{PbS}$ ,  $\text{CdSe}$ , and  $\text{ZnS}$ —exhibit obvious enhancement of structural stability compared with the corresponding bulk materials due to higher surface energy [16–19]. However, for our 23 nm  $\text{CaF}_2$  nanocrystals, the higher surface energy does not contribute to the improvement of structural stability. To the best of our knowledge, defects are considered to be one of the most important factors to affect the transition pressure of nanomaterials. In order to prove our deduction, we present the HRTEM image of the 23 nm  $\text{CaF}_2$  nanocrystals at ambient condition in Figure 6. It is clear that our sample contains visible structural impurities like dislocations and defects. These dislocations and defects could act as the weak points and induce stress concentration, so a new high-pressure phase prefers to nucleate at such defect sites. Therefore, 23 nm  $\text{CaF}_2$  nanocrystals with structural defects has a reduced nucleation pressure. The distortions and defects of the crystal structure play a dominant role in the structural stability. Wang et al. [19] studied bulk and nano  $\text{ZnS}$  using synchrotron X-ray diffraction and found that when the grain size is larger than 15 nm, the hosted defect acts to behave similarly to that in bulk; below 15 nm, the defect activities turn silent, and surface energy begins directing the enhancement of structural stability. This high-pressure research on  $\text{ZnS}$  nanomaterials is similar to our studies on  $\text{CaF}_2$  nanomaterials.

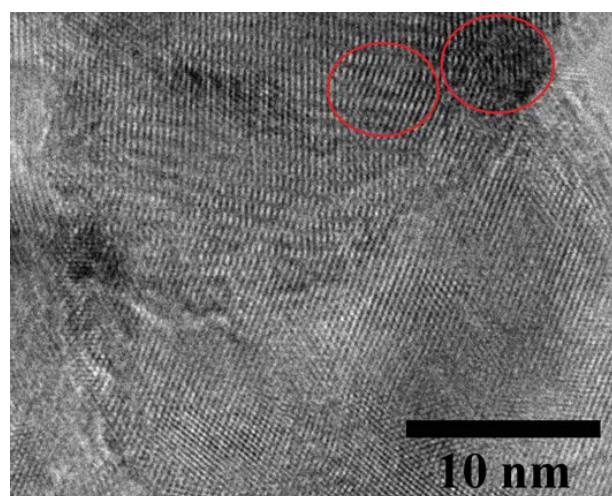


**Figure 6.** HRTEM image of the as-synthesized 23 nm  $\text{CaF}_2$  nanocrystals.

#### 4. Conclusions

The structural phase transition and compressibility of CaF<sub>2</sub> nanocrystals with size of 23 nm under high pressure were investigated by synchrotron X-ray diffraction measurement. A pressure-induced fluorite to  $\alpha$ -PbCl<sub>2</sub>-type phase transition starts at 9.5 GPa and completes at 20.2 GPa. The phase-transition pressure is lower than previously reported that of 8 nm CaF<sub>2</sub> nanocrystals and closes to bulk CaF<sub>2</sub>. Upon decompression, the fluorite and  $\alpha$ -PbCl<sub>2</sub>-type structure co-exist at ambient pressure. The bulk modulus  $B_0$  of the 23 nm CaF<sub>2</sub> nanocrystals for the fluorite and  $\alpha$ -PbCl<sub>2</sub>-type phase are 103(2) and 78(2) GPa, which are both larger than those of the bulk CaF<sub>2</sub>. The enhancement of bulk modulus compared with the corresponding bulk materials is due to higher surface energy. The HRTEM image on the sample clearly shows that the as-synthesized CaF<sub>2</sub> nanocrystals contain visible dislocations and defects which act as the weak points and induce stress concentration. The distortions and defects of the crystal structure play a dominant role in structural stability.

**Author Contributions:** JingshuWang and Jihui Lang conceived and designed the experiments; Jinghan Yang, Haiying Zhao and Xiangshan Chen fabricated and characterized the sample; Tingjing Hu, Junkai Zhang and Xiaoxin Wu collaborated in XRD, TEM measurements; Jinghai Yang and Qiliang Cui analyzed the data. All authors discussed the experiment results and contributed to writing the paper.

**Acknowledgments:** Project supported by the National Natural Science Foundation of China (grant nos. 11404137, 61378085, 51608226, 21776110), 20th Five-Year Program for Science and Technology of Education Department of Jilin Province (item no. 20150221). Synchrotron XRD experiments were performed at beamline 15U1 at the Shanghai Synchrotron Radiation Facility (SSRF).

**Conflicts of Interest:** The authors declare no conflict of interest.

#### References

1. Wang, G.; Peng, Q.; Li, Y. Upconversion Luminescence of Monodisperse CaF<sub>2</sub>: Yb<sup>3+</sup>/Er<sup>3+</sup> Nanocrystals. *J. Am. Chem. Soc.* **2009**, *131*, 14200–14201. [[CrossRef](#)] [[PubMed](#)]
2. Zhang, C.; Li, C.; Peng, C.; Chai, R.; Huang, S.; Yang, D.; Cheng, Z.; Lin, J. Facile and Controllable Synthesis of Monodisperse CaF<sub>2</sub> and CaF<sub>2</sub>: Ce<sup>3+</sup>/Tb<sup>3+</sup> Hollow Spheres as Efficient Luminescent Materials and Smart Drug Carriers. *Chem. Eur. J.* **2010**, *16*, 5672–5680. [[CrossRef](#)] [[PubMed](#)]
3. Feldmann, C.; Roming, M.; Trampert, K. Polyol-Mediated Synthesis of Nanoscale CaF<sub>2</sub> and CaF<sub>2</sub>: Ce, Tb. *Small* **2006**, *2*, 1248–1250. [[CrossRef](#)] [[PubMed](#)]
4. Gerward, L.; Olsen, J.S.; Steenstrup, S.; Sbrink, S.A.; Waskowska, A. X-ray diffraction investigations of CaF<sub>2</sub> at high pressure. *J. Appl. Crystallogr.* **1992**, *25*, 578–581. [[CrossRef](#)]
5. Kavner, A. Radial diffraction strength and elastic behavior of CaF<sub>2</sub> in low-and high-pressure phases. *Phys. Rev. B* **2008**, *77*, 224102. [[CrossRef](#)]
6. Cui, S.X.; Feng, W.X.; Hua, H.Q. Structural stabilities, electronic and optical properties of CaF<sub>2</sub> under high pressure: A first-principles study. *Comput. Mater. Sci.* **2009**, *47*, 41–45. [[CrossRef](#)]
7. Wu, X.; Qin, S.; Wu, Z.Y. First-principles study of structural stabilities, and electronic and optical properties of CaF<sub>2</sub> under high pressure. *Phys. Rev. B* **2006**, *73*, 134103. [[CrossRef](#)]
8. Dorfman, S.M.; Jiang, F.; Mao, Z.; Kubo, A.; Meng, Y.; Prakapenka, V.B.; Duffy, T.S. Phase transitions and equations of state of alkaline earth fluorides CaF<sub>2</sub>, SrF<sub>2</sub>, and BaF<sub>2</sub> to Mbar pressures. *Phys. Rev. B* **2010**, *81*, 174121. [[CrossRef](#)]
9. Boulfelfel, S.E.; Zahn, D.; Hochrein, O.; Grin, Y.; Leoni, S. Low-dimensional sublattice melting by pressure: Superionic conduction in the phase interfaces of the fluorite-to-cotunnite transition of CaF<sub>2</sub>. *Phys. Rev. B* **2006**, *74*, 094106. [[CrossRef](#)]
10. Hu, T.; Cui, X.; Wang, J.; Zhong, X.; Chen, Y.; Zhang, J.; Li, X.; Yang, J.; Gao, C. The Electrical Properties of Tb-Doped CaF<sub>2</sub> Nanoparticles under High Pressure. *Crystals* **2018**, *8*, 98. [[CrossRef](#)]
11. Hu, T.; Cui, X.; Wang, J.; Zhang, J.; Li, X.; Yang, J.; Gao, C. Transport properties of mixing conduction in CaF<sub>2</sub> nanocrystals under high pressure. *Chin. Phys. B* **2018**, *27*, 016401. [[CrossRef](#)]
12. Cazorla, C.; Errandonea, D. Superionicity and polymorphism in calcium fluoride at high pressure. *Phys. Rev. Lett.* **2014**, *113*, 235902. [[CrossRef](#)] [[PubMed](#)]

13. Cazorla, C.; Errandonea, D. Giant Mechanocaloric Effects in Fluorite-Structured Superionic Materials. *Nano Lett.* **2016**, *16*, 3124–3129. [[CrossRef](#)] [[PubMed](#)]
14. Lin, Y.; Yang, Y.; Ma, H.; Cui, Y.; Mao, W.L. Compressional Behavior of Bulk and Nanorod  $\text{LiMn}_2\text{O}_4$  under Nonhydrostatic Stress. *J. Phys. Chem. C* **2011**, *115*, 9844–9849. [[CrossRef](#)]
15. Wu, H.; Wang, Z.W.; Fan, H.Y. Stress-Induced Nanoparticle Crystallization. *J. Am. Chem. Soc.* **2014**, *136*, 7634–7636. [[CrossRef](#)] [[PubMed](#)]
16. Bian, K.; Wang, Z.; Hanrath, T. Comparing the Structural Stability of PbS Nanocrystals Assembled in fcc and bcc Superlattice Allotropes. *J. Am. Chem. Soc.* **2012**, *134*, 10787–10790. [[CrossRef](#)] [[PubMed](#)]
17. Tolbert, S.H.; Alivisatos, A.P. Size Dependence of a First Order Solid-Solid Phase Transition: The Wurtzite to Rock Salt Transformation in CdSe Nanocrystals. *Science* **1994**, *265*, 373–376. [[CrossRef](#)] [[PubMed](#)]
18. Tolbert, S.H.; Alivisatos, A.P. High-Pressure Structural Transformations in Semiconductor Nanocrystals. *Annu. Rev. Phys. Chem.* **1995**, *46*, 595–626. [[CrossRef](#)] [[PubMed](#)]
19. Wang, Z.; Guo, Q. Size-Dependent Structural Stability and Tuning Mechanism: A Case of Zinc Sulfide. *J. Phys. Chem. C* **2009**, *113*, 4286–4295. [[CrossRef](#)]
20. Jiang, J.Z.; Gerward, L.; Olsen, J.S. Pressure induced phase transformation in nanocrystal  $\text{SnO}_2$ . *Scr. Mater.* **2001**, *44*, 1983–1986. [[CrossRef](#)]
21. Wang, L.; Yang, W.; Ding, Y.; Ren, Y.; Xiao, S.; Liu, B.; Sinogeikin, S.V.; Meng, Y.; Gosztola, D.J.; Shen, G.; et al. Size-Dependent Amorphization of Nanoscale  $\text{Y}_2\text{O}_3$  at High Pressure. *Phys. Rev. Lett.* **2010**, *105*, 095701. [[CrossRef](#)] [[PubMed](#)]
22. Varghese, S.; Alexei, K.; Dubrovinsky, L.S.; Mcmillan, P.F.; Prakapenka, V.B.; Shen, G.; Muddle, B.C. Size-Dependent Pressure-Induced Amorphization in Nanoscale  $\text{TiO}_2$ . *Phys. Rev. Lett.* **2006**, *96*, 135702. [[CrossRef](#)]
23. Li, Q.; Liu, B.; Wang, L.; Li, D.; Liu, R.; Zou, B.; Cui, T.; Zou, G. Pressure-Induced Amorphization and Polyamorphism in One-Dimensional Single-Crystal  $\text{TiO}_2$  Nanomaterials. *J. Phys. Chem. Lett.* **2010**, *1*, 309–314. [[CrossRef](#)]
24. Quan, Z.W.; Wang, Y.X.; Bae, I.T.; Loc, W.S.; Wang, C.Y.; Wang, Z.W.; Fang, J.Y. Reversal of Hall–Petch Effect in Structural Stability of PbTe Nanocrystals and Associated Variation of Phase Transformation. *Nano Lett.* **2011**, *11*, 5531–5536. [[CrossRef](#)] [[PubMed](#)]
25. Wang, J.; Cui, Q.; Hu, T.; Yang, J.; Li, X.; Liu, Y.; Liu, B.; Zhao, W.; Zhu, H.; Yang, L. Pressure-Induced Amorphization in  $\text{BaF}_2$  Nanoparticles. *J. Phys. Chem. C* **2016**, *120*, 12249–12253. [[CrossRef](#)]
26. Lv, H.; Yao, M.; Li, Q.; Li, Z.; Liu, B.; Liu, R.; Lu, S.; Li, D.; Mao, J.; Ji, X.; et al. Effect of Grain Size on Pressure-Induced Structural Transition in  $\text{Mn}_3\text{O}_4$ . *J. Phys. Chem. C* **2012**, *116*, 2165–2171. [[CrossRef](#)]
27. Wieligor, M.; Wang, Y.; Zerda, T.W. Raman spectra of silicon carbide small particles and nanowires. *J. Phys. Condens. Matter* **2005**, *17*, 2387–2395. [[CrossRef](#)]
28. Wang, Y.; Zhang, J.; Wu, J.; Coffey, J.L.; Lin, Z.; Sinogeikin, S.V.; Yang, W.; Zhao, Y. Phase transition and compressibility in silicon nanowires. *Nano Lett.* **2008**, *8*, 2891–2895. [[CrossRef](#)] [[PubMed](#)]
29. Wang, Y.; Zhang, J.; Zhao, Y. Strength weakening by nanocrystals in ceramic materials. *Nano Lett.* **2007**, *7*, 3196–3199. [[CrossRef](#)] [[PubMed](#)]
30. Senter, R.A.; Pantea, C.; Wang, Y.; Liu, H.; Zerda, T.W.; Coffey, J.L. Structural Influence of Erbium Centers on Silicon Nanocrystal Phase Transitions. *Phys. Rev. Lett.* **2004**, *93*, 175502. [[CrossRef](#)] [[PubMed](#)]
31. Wu, J.; Coffey, J.L.; Wang, Y.; Schulze, R. Oxidized Germanium as a Broad-Band Sensitizer for Er-Doped  $\text{SnO}_2$  Nanofibers. *J. Phys. Chem. C* **2009**, *113*, 12–16. [[CrossRef](#)]
32. Wang, Y.; Zhao, Y.; Zhang, J.; Xu, H.; Wang, L.; Luo, S.; Daemen, L. In situ phase transition study of nano- and coarse-grained  $\text{TiO}_2$  under high pressure/temperature conditions. *J. Phys. Condens. Matter* **2008**, *20*, 125224. [[CrossRef](#)]
33. Wang, Y.; Yang, W.; Zou, G.; Wu, J.; Coffey, J.L.; Sinogeikin, S.V.; Zhang, J. Anomalous Surface Doping Effect in Semiconductor Nanowires. *J. Phys. Chem. C* **2017**, *121*, 11824–11830. [[CrossRef](#)]
34. Wang, J.; Hao, J.; Wang, Q.; Jin, Y.; Li, F.; Liu, B.; Li, Q.; Liu, B.; Cui, Q. Pressure-induced structural transition in  $\text{CaF}_2$  nanocrystals. *Phys. Status Solidi B* **2011**, *248*, 1115–1118. [[CrossRef](#)]
35. Birch, F. Finite Strain Isotherm and Velocities for Single-Crystal and Polycrystalline NaCl at High Pressures and 300 K. *J. Geophys. Res.* **1978**, *83*, 1257–1268. [[CrossRef](#)]
36. Wang, J.; Ma, C.; Zhou, D.; Xu, Y.; Zhang, M.; Gao, W.; Zhu, H.; Cui, Q. Structural phase transitions of  $\text{SrF}_2$  at high pressure. *J. Solid State Chem.* **2012**, *186*, 231–234. [[CrossRef](#)]

37. Popescu, C.; Sans, J.A.; Errandonea, D.; Segura, A.; Villanueva, R.; Sapiña, F. Compressibility and structural stability of nanocrystalline TiO<sub>2</sub> anatase synthesized from freeze-dried precursors. *Inorg. Chem.* **2014**, *53*, 11598–11603. [[CrossRef](#)] [[PubMed](#)]
38. Grinblat, F.; Ferrari, S.; Pampillo, L.G.; Saccone, F.; Errandonea, D.; Santamaria-Perez, D.; Segura, A.; Vilaplana, R.; Popescu, C. Compressibility and structural behavior of pure and Fe-doped SnO<sub>2</sub> nanocrystals. *Solid State Sci.* **2017**, *64*, 91–98. [[CrossRef](#)]
39. Hall, E.O. The Deformation and Ageing of Mild Steel: III Discussion of Results. Proceedings of the Physical Society. *Sect. B* **1951**, *64*, 747. [[CrossRef](#)]
40. Petch, N. The cleavage strength of polycrystals. *J. Iron Steel Inst.* **1953**, *174*, 25–28.
41. Angel, R.J. The high-pressure, high-temperature equation of state of calcium fluoride, CaF<sub>2</sub>. *J. Phys. Condens. Matter* **1993**, *5*, L141. [[CrossRef](#)]



© 2018 by the authors. Licensee MDPI, Basel, Switzerland. This article is an open access article distributed under the terms and conditions of the Creative Commons Attribution (CC BY) license (<http://creativecommons.org/licenses/by/4.0/>).